Koopman-Based Modeling of an Open Cathode Proton Exchange Membrane Fuel Cell Stack

Abstract: Accurate modeling is crucial for the effective design and control of fuel cell stacks. Although physics-based models are widely used, data-driven methods such as the Koopman operator have not been fully explored for fuel cell modeling. In this paper, a Koopman-based approach is utilized to model the thermal dynamics of a 5 kW open cathode proton exchange membrane fuel cell stack. A physics-based model is used as the baseline for comparison. By varying the cooling fan rotational speed, the dynamics of the fuel cell stack were measured from the low load of near 0 kW to about 5 kW. Compared to experimental results, the steady-state absolute errors of Koopman-based models are within 3%. Additionally, once given sufficient dimension, the development effort required for the Koopman-based model is relatively low compared to the traditional physics-based approach, while still achieving a high level of accuracy. These findings suggest the Koopman operator may be a suitable alternative approach for fuel cell stack modeling that enables the development of more accurate and efficient modeling methods for fuel cell systems and facilitates the implementation of the linear optimal algorithms.

Keywords: open-cathode proton exchange membrane (PEM) fuel cell (FC), data-driven modeling, Koopman operator, physics-based modeling, control-oriented modeling.

1. INTRODUCTION

The demand for energy continues to rise, driven by the growth of industrialization and urbanization worldwide. Traditional energy sources such as fossil fuels have been the primary source of energy for many years, but they are associated with several environmental problems, such as air pollution, greenhouse gas (GHG) emissions, and climate change. According to the US Environmental Protection Agency, the majority of GHG emissions from the transportation sector are carbon dioxide (CO_2) emissions resulting from the combustion of petroleum-based products such as gasoline and diesel fuel in internal combustion engines (ICE) [EPA (2023)]. The hydrogen fuel cell (FC) is considered a promising alternative to traditional power sources due to its high efficiency and low emissions. Through an electrochemical reaction, fuel cells produce only water and heat as byproducts. This characteristic makes hydrogen fuel cells an environmentally friendly option for energy generation. In particular, hydrogen fuel cell stacks have been widely studied as a means of producing electrical power for a variety of applications, from small portable devices to large-scale stationary power generation.However, it is challenging to precisely simulate and predict the behavior of the stack under varying operating conditions due to the intricate electrochemical and transport processes that take place within it.

Over the years, various modeling methods have been developed to enhance the prediction of the performance of FC stacks, and a thorough review of these methods can be found in [Wu (2016); Yang et al. (2020)]. The study in [Pukrushpan et al. (2002)] presented a physics-based dynamic model with a focus on addressing the airflow control issue. In [Hillstrom et al. (2013)], a physics-based model is developed for a 540 kW power output high-speed vehicle to predict the pressure dynamics at high current density conditions. Artificial neural network (ANN) approaches have also been utilized as in [Barzegari et al. (2019)] in which an ANN was utilized as a data-driven method for modeling a 400 W FC stack. However, since this kind of approach is non-linear in nature, it requires computationally intensive non-linear optimal algorithms or the linearization of the model before utilizing linear optimal algorithms. Additionally, as the complexity of the neural network structure grows, the training cost increases exponentially. Nevertheless, the potential of the Koopman operator approach as a data-driven alternative for modeling FC stacks has not been thoroughly investigated.

The concept of Koopman operator, representing a nonlinear dynamical system using an infinite-dimensional linear operator, dates back to the pioneering works of Koopman in the early 1930s [Koopman (1931)]. In general, the Koopman operator, an infinite-dimensional linear operator, represents a linear transformation that acts on non-linear observable functions of a dynamical system into a higher-dimensional space, and it has since been studied by many researchers [Mauroy et al. (2020); Budišić et al. (2012)]. In [Williams et al. (2015)], extended dynamic mode decomposition (EDMD) was introduced as a method capable of approximating the infinite-dimensional Koopman operator to a finite-dimension. The fact that the Koopman-based model is linear means that it can be directly integrated into linear model-based optimization algorithms, which are computationally efficient compared to nonlinear optimization algorithms. This makes the Koopman operator superior compared to other data-driven techniques [Korda and Mezić (2018)].

The primary contribution of this paper is the pioneering application of the Koopman operator to model the FC stack dynamic system. Our findings highlight the potential of the Koopman-based approach by comparing it with the physics-based model. These insights provide a pathway

toward developing a more accurate and efficient control-oriented modeling approach for FC stacks. The paper introduces the experimental setup and test conditions in Section 2 and present the physics-based model and Koopman-based model, and analyze their calibration and training results using the same datasets. In section 4, we compare and analyze the performance of the physics-based model and Koopman-based model with a different dataset than the ones used in Section 3. Section 5 provides some brief concluding remarks and introduces our future research directions.

2. EXPERIMENTAL CONFIGURATION

2.1 Experimental Setup

In this study, a 5kW open-cathode proton exchange membrane (PEM) fuel cell stack manufactured by Horizon is utilized. Specifications of the fuel cell stack are summarized in Table 1 and the layout of the experimental set up is shown in Figure 1. To monitor the ambient conditions, a hygrometer is used to measure the temperature and relative humidity. The compressed hydrogen gas is supplied to the anode side of the FC stack through a regulator and a flow control valve. The cathode side of the FC stack is exposed to the ambient air with 81 channels per cell. A purge valve is used to purge the unused hydrogen, back diffused water and nitrogen gas every 10 seconds.

Table 1. Fuel Cell Stack Specifications

Description	Value	Unit
Minimum fuel cell voltage	60	V
Maximum fuel cell stack current	90	A
Maximum fuel cell stack temperature	65	°C
External power supply	24/8-12	V/A
Number of cells	120	-
Active area per cell	150	cm^2

The FC stack is equipped with four 25kHz fans (San Ace 9SG5724P5H61) that provide oxygen supply and cooling. Their rotational speed was dictated by an Arduino controller with the speed being manipulated by pulse width modulation (PWM). To simulate the loads on the FC stack, a Chroma electronic load (63206A-150-600), with a capacity of 6 kW, is employed. The electronic load is capable of adjusting the current load. A Chroma DC power supply (62006P-100-25) provides a constant voltage to the built-in controller and the fans.

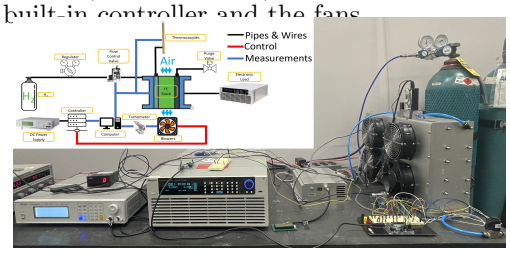

Fig. 1. Experimental setup schematic

Data acquisition is conducted via several devices. The FC stack built-in module logs stack output voltage, current, and in-stack temperature. A tachometer (8518T96) and a panel-meter (8518T61) are used to measure the fans rotational speed and anode intake pressure is recorded by an Aalborg (DPC47) flow control valve.

2.2 Operating Conditions

The equipment went through a 30-minute warm-up period before data collection and each test condition was held for about five minutes to ensure the system reached steady state. Data for the last one minute were averaged to get the steady-state values. A polarization test was conducted under default operating conditions where the FC stack was controlled and supervised by the built-in controller, and only the current load was varied. The current load for the polarization test ranges from 0A to 90A, with different intervals for each load range. At low and high loads where the gradient of the voltage to the current is relatively larger, a smaller interval was applied. To study the thermal effects, a set of tests with varying fan speed were conducted in which the fans were operated from a minimum of 1500 rpm to a maximum of 5800 rpm through the PWM signal from the self-built controller. Four current sweeps with fan speeds were conducted, and the speed was kept constant for each test set. The FC stack temperatures at steady-state versus the current loads are demonstrated in Figure 2. As the figure shows, test sets 1 and 2 have fewer points than test sets 3 and 4, because the system's short circuit unit (SCU) protection is activated due to the fan's reduced cooling capacity at lower speeds which drives the stack temperature above the upper limit. The polarization test and data sets 1, 2 and 3 are used as calibration data sets for the physics-based model and as training data sets for the Koopman-based model. Data set 4, which has a different PWM and additional loads that are not covered by the other data sets, is used to validate both models.

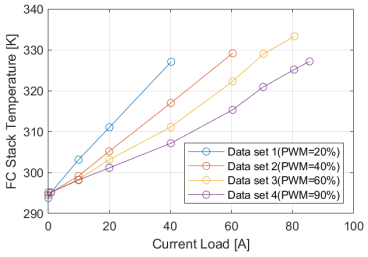

Fig. 2. Experimental data of the FC stack temperature

3. MODELING

In this section, the physics-based model and the Koopman-based model and their calibration are discussed.

3.1 Physics-based model

The FC stack physics-based model has three submodels: the electro-chemical model, thermal model, and hydrogen inlet pressure model as illustrated in Figure 3. The physics-based model has four input variables: FC stack temperature, current load, hydrogen inlet pressure, and PWM signal. It produces two outputs: FC stack temperature and voltage. The polarization curve test data was utilized for calibrating the electrochemical model, while data set 1, 2, and 3 were used for calibrating the thermal model and hydrogen inlet pressure model.

Electrochemical Model Fuel cells are electrochemical devices that convert chemical energy directly into electrical energy via electrochemical reactions shown as Equation 1:

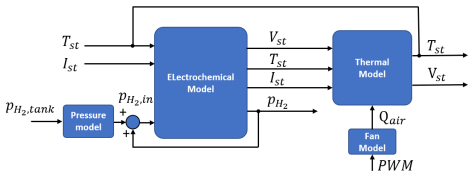

Fig. 3. Physics-based model schematic

$$\begin{aligned} &\text{Anode: } H_2 \rightarrow 2H^+ + 2e^- \\ &\text{Cathode: } \frac{1}{2}O_2 + 2H^+ + 2e^- \rightarrow H_2O \\ &\text{Overall: } H_2 + \frac{1}{2}O_2 \rightarrow H_2O \end{aligned} \tag{1}$$

The total FC stack voltage V_{st} is the product of the total number of fuel cells (N_{st}) and the voltage output of a single cell (V_{cell}). Generally, the fuel cell output voltage can be expressed as Equation 2:

$$V_{cell}(t) = V_{oc}(t) - V_{act}(t) - V_{ohm}(t) - V_{con}(t) \tag{2}$$

where V_{oc} is the open circuit voltage; V_{act}, V_{ohm} and V_{con} are the activation loss, ohmic loss, and concentration loss, respectively. The open circuit cell voltage of a FC stack is the voltage output when there is no external load connected to the system and it varies with temperature, pressure, and activity under non-standard conditions and can be written as Equation 3 [O'hayre et al. (2016)]:

$$\begin{aligned} V_{oc}(t) = E^0 &+ \frac{\Delta s(T_{st})}{nF}(T_{st}(t) - T_{amb}) \\ &- \frac{RT_{st}(t)}{nF} ln \frac{1}{p_{H_2(t)} p_{O_2}^{1/2}} \end{aligned} \tag{3}$$

where the E^0 is the non-standard reversible voltage, Δs is the sensible entropy, T_{st} is the fuel cell stack temperature, T_{amb} is the ambient temperature, R is the ideal gas constant, n is the number of moles of electrons transferred from the hydrogen gas and equal to 2, F is Faraday's constant, p_{H_2} is the hydrogen inlet pressure, and p_{O_2} is the oxygen inlet pressure and is equal to ambient air pressure multiplied by the oxygen fraction of the air. The non-standard reversible voltage E^0 is given by:

$$E^0 = -\frac{\Delta g(T_{st})}{nF} \tag{4}$$

where Δg is the non-standard-state free-energy change for the reaction [Kyle (1984)].

The activation loss can be calculated from Equation 5:

$$V_{act}(t) = \frac{RT_{st}(t)}{\alpha nF} log\left(\frac{i(t)}{i_0}\right) \tag{5}$$

where i is the current density of the FC stack, i_0 is the exchange current density, α is the charge transfer coefficient and is set to 0.5 here. The ohmic voltage loss is given by Equation 6:

$$V_{ohm}(t) = i(t)R_{ohm} = i(t)(R_{ion} + R_{elec}) \tag{6}$$

where R_{ohm} is the total ohmic resistance, R_{ion} is the ionic charge transport resistance, R_{elec} is the electronic charge transport resistance and equal to 0.00007Ω. Since a 30-minute warm-up test is conducted prior to each experimental test, it is assumed that the membrane is fully self-humidified due to this warm-up process. The value of R_{ion} can be obtained by utilizing Equation 7 as presented in [Wang et al. (2014)]:

$$R_{ion} = \frac{181.6[1 + 0.03i(t) + 0.062(\frac{T_{st}(t)}{303})^2 i^{2.5}(t)]l}{[\lambda_m - 0.634 - 3i(t)]exp[4.18(1 - \frac{303}{T_{st}(t)})]A} \tag{7}$$

where l is the membrane thickness (0.0035 cm), λ_m denotes the water content of the membrane (22), and A represents the active area (150 cm^2). The concentration voltage loss is given by [Hao et al. (2016)] :

$$V_{conc} = m(exp^{ni(t)} - 1) \tag{8}$$

where the coefficients of m and n are determined through curve fitting to the experimental polarization data.

Figure 4 demonstrates the results of the electrochemical model predictions for the polarization curve. The steady-state absolute errors are within 3%. Furthermore, within the current load range of 0A to approximately 57A, relatively larger errors are observed compared to the high-load region. These errors can be attributed to the activation voltage loss and ohmic voltage loss models, which primarily impact the low and medium current load regions.

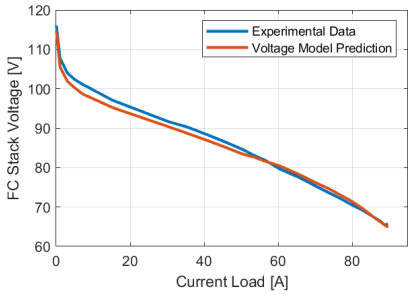

Fig. 4. Polarization curve comparison

Thermal model The FC stack thermal dynamics can be described as following Equation 9 [Ishaku et al. (2014)]

$$C_t \frac{dT_{st}(t)}{dt} = P_{tot}(t) - P_{st}(t) - \dot{Q}_{coolant}(t) \tag{9}$$

where P_{tot} is the total power released by the electrochemical reactions (W), P_{st} represents the electrical power output of the FC stack (W), and $\dot{Q}_{coolant}$ is the heat dissipated to the cooling airflow. C_t is the thermal capacitance (J/K-s) determined by data observation. Since the built-in controller and the fans are powered by a separate DC power supply rather than consuming power generated by the FC stack in the tests, their power consumption is not considered in this equation. The total power released by the electrochemical reaction in the FC stack can be calculated from Equation 10:

$$P_{tot} = \frac{N_{st} I_{st}(t) \Delta h}{nF} \tag{10}$$

where Δh represents the higher heating value of the hydrogen gas. The FC stack output power is the product of the stack voltage ($V_{st}(t)$) and stack current ($(t)I_{st}(t)$).

The variable $\dot{Q}_{coolant}$ is determined by considering the air blowing through the FC stack, and can be derived from:

$$\dot{Q}_{coolant} = \eta_{fan} \dot{m}_{air}(t) c_p (T_{st}(t) - T_{amb}) \tag{11}$$

where η_{fan} is the fan efficiency, $\dot{m}_{air}$ is the air mass flow rate, and c_p is the specific heat coefficient of the air. To obtain the air mass flow rate in the above equation, its volumetric flow rate for any rotational speed of the fan is given by Equation 12:

$$Q(t) = \omega(t)\frac{Q_{nom}}{\omega_{nom}} \tag{12}$$

where ω is the arbitrary fan speed (RPM), Q_{nom} is the nominal volumetric flow rate (m^3/s) of the fan, and ω_{nom} is the nominal fan speed (RPM) at the operating curve, Q_{norm} and ω_{norm} are obtained based on the method in [Ishaku et al. (2014)]. A static empirical model is employed to describe the correlation between the input PWM command to the fans' rotational speed:

$$\omega(t) = \begin{cases} 1500 & \text{for PWM}\in[0,20) \\ 60.36u_{fan}(t) + 294.2 & \text{for PWM}\in[20,90) \\ 5800 & \text{for PWM}\in(90,100] \end{cases} \tag{13}$$

where u_{fan} is the PWM of fan.

Data sets 1, 2, and 3 are used for model calibration. To determine η_{fan}, MATLAB fminsearch function is used and the output is 46.59%. Data set 4 is used to validate the thermal model. Figure 5 shows the thermal model calibration results, and the errors are within 3% for all the test conditions. To enable control of the transient response, all responses are assumed to be first-order, and 5209 (J/K-s) is assigned to C_t based on experimental data.

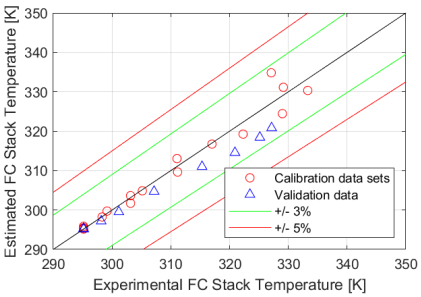

Fig. 5. Fan efficiency calibration results

Hydrogen Inlet Pressure Model As a result of a water concentration gradient across the membrane, water molecules generated in the cathode can diffuse back to the anode. Similarly, nitrogen molecules present in the cathode air stream can transfer to the anode side due to a corresponding nitrogen concentration gradient. Consequently, water and nitrogen molecules tend to accumulate in the anode channels and can impede hydrogen delivery leading to voltage losses and degradation [O'hayre et al. (2016)]. To prevent this phenomenon, a periodic anode purging is performed. During the purging process, the back diffused nitrogen gas and water, along with unused hydrogen gas are removed from the anode, resulting in improved performance. The period of the purging cycle is fixed at 10 seconds, while the purging time varies and is determined based on a lookup table that takes into account the current load and temperature of the FC stack. Equation 14 [Ishaku et al. (2014)] can be utilized to determine the hydrogen gas inlet pressure

$$\begin{aligned} p_{H_2,inlet}(t) =& p_{tank}(t)u(t) - \Delta p_{purge}u(t-t_1) \\ &+ \Delta p_{purge}(1 - e^{-\frac{t-t_2}{\tau_p}}) \end{aligned} \tag{14}$$

where p_{tank} is the hydrogen tank outlet pressure, Δp_{purge} and τ_P is the pressure drop during the purging and time constant, respectively, and they are determined from the data. The time instances t_1 and t_2 refer to the start and the end of the purging process, respectively, and $u(t)$ is the unit step function. Though the hydrogen tank outlet pressure is predetermined as a constant, an increase in current load will lead to a higher hydrogen mass flow rate, causing a drop in the hydrogen tank pressure. As such, p_{tank} is modeled as a third order polynomial of the stack current load.

Figure 6 shows the hydrogen gas inlet pressure results of data set 2. It is clear that this model can capture the pressure drops caused by changing the current load and the purge valve status. Some misalignment of the pressure drop can be observed, and this this is caused by a sensor sampling time which is too long to capture the transient changes. In addition, during each purging cycle, there is an additional pressure drop caused by the SCU which also consumes the hydrogen gas. The SCU's purpose is to safeguard from overload, overvoltage, and overheating.

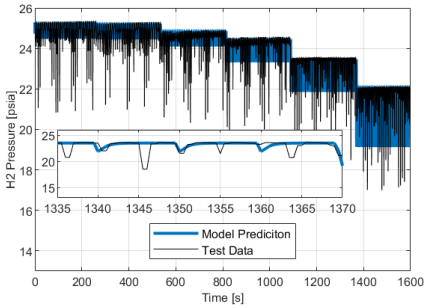

Fig. 6. Purging result at 40%PWM (Data set 2)

3.2 Data-Driven Model

Koopman concepts The Koopman operator is applied to a discrete-time nonlinear dynamic system with the form:

$$\boldsymbol{x}_{k+1} = f(\boldsymbol{x}_k, \boldsymbol{u}_k) \tag{15}$$

where k represents the current time step, $\boldsymbol{x} \in \mathbb{R}^n$ denotes the state of the dynamic system with n dimensions, $\boldsymbol{u} \in \mathbb{R}^m$ is the control input with m dimensions, f is the nonlinear transition mapping.

The Koopman operator, $\mathcal{K}$:$\mathcal{F} \rightarrow \mathcal{F}$, is a linear operator (typically infinite-dimensional) acting on nonlinear observable functions $\psi : \mathbb{R}^n \rightarrow \mathbb{R}^N$ which belong to $\mathcal{F}$. $\mathcal{F}$ is a space of observables that is invariant under the action of the Koopman operator, and it can be expressed as:

$$(\mathcal{K}\psi)(x) = \psi(f(x)) \tag{16}$$

In this study, the goal is to construct a control-oriented model for the FC stack by using the Koopman operator. To achieve this, extended dynamic mode decomposition (EDMD) [Williams et al. (2015)] is applied to approximate the infinite-dimension Koopman operator into a finite-dimension form $\mathcal{K} \in \mathbb{R}^N$, N≫n. In general, it performs regression on a vector of observable functions and produces the lifted state vector.

The lifted state $\boldsymbol{z} \in \mathbb{R}^N$ can be expressed as:

$$\boldsymbol{z} = \phi(\boldsymbol{x}) = [\phi_1(\boldsymbol{x}), \phi_2(\boldsymbol{x}) ... \phi_N(\boldsymbol{x})]^T \tag{17}$$

and the discrete-time of the lifted state space is given by:

$$\begin{aligned} z_{k+1} &= Az_k + Bu_k \\ \hat{x}_k &= Cz_k \end{aligned} \tag{18}$$

where $\hat{x}$ denotes the predicted states, the best-fit linear operators A, B and C are obtained through EDMD, and $A \in \mathbb{R}^{N\times N}$, $B \in \mathbb{R}^{N\times m}$, $C \in \mathbb{R}^{n\times N}$.

For the discrete system, the data has inputs to the Koopman operator that include the current state ($\chi \in \mathbb{R}^{n\times k}$), successor state ($\chi^+ \in \mathbb{R}^{n\times k}$) and control inputs ($U \in \mathbb{R}^{m\times k}$). The matrices Z and Z^+ are composed of the lifted states with the dimension $\mathbb{R}^{N\times k}$.

The matrices of A, B and C can be obtained through the best least-squares, and the analytical solutions can be expressed as:

$$\begin{aligned}[A, B] &= Z^+[Z, U]^\dagger \\ C &= \chi Z^\dagger\end{aligned} \tag{19}$$

where † denotes the Moore-Penrose pseudoinverse of a matrix. In addition, the thin plate spline radial basis function (RBF) is used:

$$\varphi(r) = r^2 ln(r) \tag{20}$$

where r represents the distance between the data point to randomly generated centers.

In this study, the state inputs were temperature, voltage and hydrogen pressure. The control inputs were load and PWM command and the outputs were temperature, voltage and hydrogen pressure. As such, the lifted states of Eq.17 can be summarized as:

$$\boldsymbol{z} = [x_1, x_2, x_3, \phi_4(\boldsymbol{x}), ..., \phi_N(\boldsymbol{x})]^T \tag{21}$$

where $\phi_N(\boldsymbol{x})$ represents the radial basis function (RBF) with N $\geq$ 4, by defining the lifted states in the proposed format, the C matrix in Eq.18 can be obtained easily. Furthermore, in combination with the A and B matrices, it can be iterated through Eq.18.

To determine the optimal hyperparameters for the Koopman-based model, two Koopman operators with different dimensions (N=9 and N=13) were trained and evaluated. The model with the lowest overall root mean square error (RMSE) was selected as the optimal model. This optimal model was then compared to the physics-based model in Section 4. The 9-dimensional Koopman-based model was chosen for comparison due to its comparable accuracy to the 13-dimensional model but with reduced computational time (14.84s vs. 32.24s).

4. RESULTS

In this section, we will analyze and compare the performance of the physics-based model and the Koopman-based model using data set 4 with fan's PWM of 90%, which has never been used for model calibration. The prediction horizon of Koopman-based model was set as 5 sample time steps to reduce the accumulated errors. Figure 7 compares the voltage transient results obtained from the 9-dimensional Koopman-based model (Koopman9) and the physics-based model. At steady-state conditions, the Koopman-based model has lower errors under all test conditions though the absolute errors of both models are less than 3%. Meanwhile, the Koopman-based model demonstrates superior performance in capturing transient dynamics compared to the physics-based model. The limitation arises from the thermal model's first-order nature, as evident from Eq.9. Consequently, the electrochemical model follows the dynamics of the thermal model, which cannot fully capture the non-linear dynamic behavior of the FC stack voltage. This limitation becomes more evident in high-load regions.

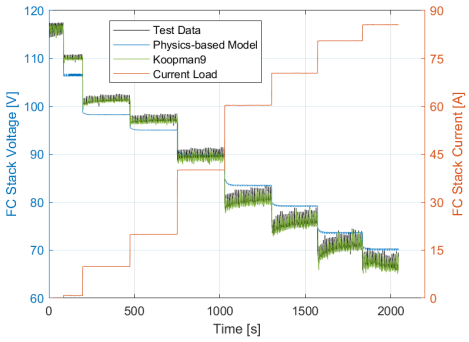

Fig. 7. Voltage output comparison at maximum fan speed (Data set 4)

The Koopman-based model has a smaller error range and a more concentrated error distribution compared to the physics-based model. The maximum error of the physics-based model is 6.68 Volts, which occurred during the transient processes as shown in Figure 7 due to the limitation of the first-order thermal model. In addition, the error distribution observed in Figure 7 exhibits slight differences compared to Figure 4. Specifically, in Figure 4, the voltage is over-estimated after approximately 57A, whereas in Figure 7, this overestimation occurs after 40A. This variation can be attributed to the maximum fan speed causing in lower in-stack temperature.

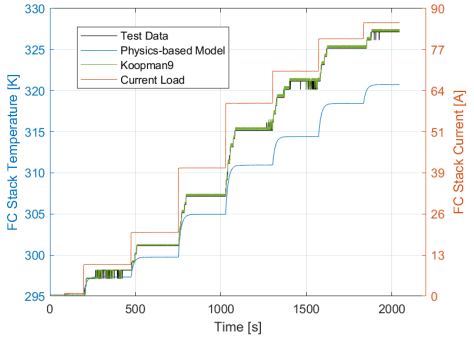

Fig. 8. Stack temperature comparison at maximum fan speed (Data set 4)

Figure 8 shows the FC stack temperature prediction results. Similar to the voltage results, Koopman-based model demonstrates better transient and steady state performance compared to the physics-based model, with a reduced error range and more concentrated error distribution. The physics-based model underestimated stack temperature for all test conditions. This is because the physics-based coolant model is based on a constant efficiency for the fan, which was overestimated based on data sets 1, 2, and 3. As a result, it led to an underestimation of the stack temperature for data set 4 with 90% PWM, with the maximum error of 6.4 K at the load of 85 A. One possible approach to enhance the accuracy of the temperature prediction of the physics-based model is by modeling the fan's efficiency as a function of PWM instead of a constant. However, this would result in increased complexity and computational cost of the model. Although the

physics-based model has overestimated temperature, both the Koopman-based and physics-based models exhibit an error within 3%.

Figure 9 compares the prediction results and the error distributions of the FC stack hydrogen inlet pressure between the physics-based model and the Koopman-based model. Both models exhibit a steady-state error within 3%, despite the transient overestimation observed in the Koopman-based model's error. The overall error distribution across all of the validation data are within 2 psia. It can be observed that the Koopman-based model shows a slight overestimation of the hydrogen inlet pressure for all validation conditions. This is because the calibration data sets are with PWM up to 60%, while that of the validation data set is 90%. A possible way to optimize this is that make the H2 pressure weight larger during the training process. Similar to the calibration results, the misalignment of the pressure drop is observed, which needs improvement in the future. The computation time of the physics-based model is 0.2205 seconds compared to 0.1486 seconds for the Koopman-based model. As such, the Koopman-based model has a computational time that is 36.64% less than the physics-based model.

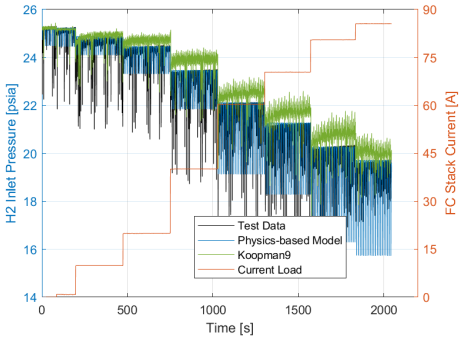

Fig. 9. Hydrogen pressure results at maximum fan speed (Data set 4)

5. CONCLUSIONS AND FUTURE WORK

In this study, a Koopman-based model was developed for a PEM fuel cell stack and its performance was compared to a baseline physics-based approach. Both models were calibrated with the experimental data collected under a wide range of operating conditions, with sweeps of current load and fan's PWM. Based on the test results of the stack voltage, temperature, and hydrogen inlet pressure, it is clear that the Koopman-based model can capture transient dynamics without requiring additional effort. In addition, the Koopman-based model can have a faster computational speed than the physics-based model. Compared to the traditional physics-based approach, the development effort required for the Koopman-based model is relatively low but with high accuracy. Future work will focus on the systematic determination of the optimal hyperparameters and radial basis function for the Koopman-based modeling approach. Modeling and control of temperature and humidity variations within the FC stack will also be explored.

REFERENCES

Barzegari, M.M., Rahgoshay, S.M., Mohammadpour, L., and Toghraie, D. (2019). Performance prediction and analysis of a dead-end pemfc stack using data-driven dynamic model. *Energy*, 188, 116049.

Budišić, M., Mohr, R., and Mezić, I. (2012). Applied koopmanism. *Chaos: An Interdisciplinary Journal of Nonlinear Science*, 22(4), 047510.

EPA (2023). Overview of greenhouse gases. https://www.epa.gov/ghgemissions/overview-greenhouse-gases, last accessed 01 March 2023.

Hao, D., Shen, J., Hou, Y., Zhou, Y., and Wang, H. (2016). An improved empirical fuel cell polarization curve model based on review analysis. *International Journal of Chemical Engineering*, 2016.

Hillstrom, E.T., Canova, M., Guezennec, Y., and Rizzoni, G. (2013). Modeling the cathode pressure dynamics in the buckeye bullet ii 540 kw hydrogen pem fuel cell system. *Journal of power sources*, 241, 33–45.

Ishaku, J., Lotfi, N., Zomorodi, H., and Landers, R.G. (2014). Control-oriented modeling for open-cathode fuel cell systems. In *2014 American Control Conference*, 268–273. IEEE.

Koopman, B.O. (1931). Hamiltonian systems and transformation in hilbert space. *Proceedings of the National Academy of Sciences*, 17(5), 315–318.

Korda, M. and Mezić, I. (2018). Linear predictors for nonlinear dynamical systems: Koopman operator meets model predictive control. *Automatica*, 93, 149–160.

Kyle, B.G. (1984). Chemical and process thermodynamics.

Mauroy, A., Susuki, Y., and Mezić, I. (2020). *Koopman operator in systems and control*. Springer.

O'hayre, R., Cha, S.W., Colella, W., and Prinz, F.B. (2016). *Fuel cell fundamentals*. John Wiley & Sons.

Pukrushpan, J., Stefanopoulou, A., and Peng, H. (2002). Modeling and control for pem fuel cell stack system. In *Proceedings of the 2002 American Control Conference (IEEE Cat. No.CH37301)*, volume 4, 3117–3122 vol.4. doi:10.1109/ACC.2002.1025268.

Wang, Y.X., Yu, D.H., Chen, S.A., and Kim, Y.B. (2014). Robust dc/dc converter control for polymer electrolyte membrane fuel cell application. *Journal of Power Sources*, 261, 292–305.

Williams, M.O., Kevrekidis, I.G., and Rowley, C.W. (2015). A data–driven approximation of the koopman operator: Extending dynamic mode decomposition. *Journal of Nonlinear Science*, 25, 1307–1346.

Wu, H.W. (2016). A review of recent development: Transport and performance modeling of pem fuel cells. *Applied energy*, 165, 81–106.

Yang, B., Wang, J., Zhang, M., Shu, H., Yu, T., Zhang, X., Yao, W., and Sun, L. (2020). A state-of-the-art survey of solid oxide fuel cell parameter identification: Modelling, methodology, and perspectives. *Energy Conversion and Management*, 213, 112856.